Reduced air–sea CO_2 exchange in the Atlantic Ocean due to biological surfactants

Ryan Pereira, Ian Ashton, Bita Sabbaghzadeh, Jamie D. Shutler & Robert C. Upstill-Goddard

Nature Geoscience doi:10.1038/s41561-018-0136-2

Published: 28 May 2018

https://www.nature.com/articles/s41561-018-0136-2

Author Information

Affiliations

The Lyell Centre, Heriot-Watt University, Edinburgh, EH14 4AP

Ryan Pereira

University of Exeter, Cornwall, TR10 9EZ

Ian Ashton & Jamie D. Shutler

School of Natural and Environmental Sciences, Newcastle University, Newcastle NE1 7RU

Robert Upstill-Goddard & Bita Sabbaghzadeh

Corresponding Author

Ryan Pereira, The Lyell Centre, Heriot-Watt University, Edinburgh, EH14 4AP

(r.pereira@hw.ac.uk)

Abstract

Ocean CO_2 uptake accounts for 20–40% of the post-industrial sink for anthropogenic CO_2. The uptake rate is the product of the CO_2 interfacial concentration gradient and its transfer velocity, which is controlled by spatial and temporal variability in near surface turbulence. This variability complicates CO_2 flux estimates and in large part reflects variable sea surface microlayer enrichments in biologically derived surfactants that cause turbulence suppression. Here we present a direct estimate of this surfactant effect on CO_2 exchange at the ocean basin scale, with derived relationships between its transfer velocity determined experimentally and total surfactant activity for Atlantic Ocean surface seawaters. We found up to 32% reduction in CO_2 exchange relative to surfactant-free water. Applying a relationship between sea surface temperature and total surfactant activity to our results gives monthly estimates of spatially-resolved "surfactant suppression" of CO_2 exchange. Large areas of reduced CO_2 uptake resulted, notably around 20 °N, and the magnitude of the Atlantic Ocean CO_2 sink for 2014 was decreased by 9%. This direct quantification of the surfactant effect on CO_2 uptake at the ocean basin scale offers a framework for further refining estimates of air-sea gas exchange up to the global scale.

Surfactants and gas exchange between the atmosphere and ocean

Environmental control of the gas transfer velocity (k_w) of a sparingly soluble gas like CO_2 is exerted through the modification of turbulent diffusion at the air-sea interface [1]. Wind speed is a fundamental control of near surface turbulence but relationships between k_w estimated in situ using volatile tracers and corresponding wind speeds show considerable scatter, of which only about 50% is attributable to procedural and/or measurement errors [2]. Contrasting k_w - wind speed parameterisations have consequently been derived for different ocean regions [3, 4, 5, 6], the differences between them resulting from additional and variable k_w control by several other turbulence related variables. These include atmospheric stability, wind fetch, sea state, breaking waves, white caps, bubble transport, rain and the presence of surface active organics (surfactants) [1].

Biologically-derived surfactants[7, 8] are ubiquitous in the open ocean sea surface microlayer (SML)[9, 10], where in addition to limiting the rate of air-sea gas exchange[11], they contribute to the formation of marine boundary layer (MBL) aerosols involved in atmospheric chemistry and climate regulation[12]. The SML is <400 μm deep but is physically and biogeochemically distinct from both the underlying water and the atmosphere[13]. SML enrichments in surfactants, other dissolved components[14] and buoyant particles predominantly occur via bubble scavenging from subsurface water (SSW) [13]. Surfactants can be soluble or insoluble, the former being most important to air-sea gas exchange [7, 8, 15] by suppressing k_w through modified surface hydrodynamics and subsequent capillary-gravity wave damping [16, 17]. By contrast, insoluble surfactants that form visible "monolayer" slicks ~1-10 nm thick in calm seas, break down and disperse under increasing turbulence [18]. Soluble surfactants accumulating in the SML include transparent exopolymer particles (TEP) [19], polysaccharides [20], lipid-like material e.g. [21], amino acids [22] and chromophoric dissolved organic matter

63 (CDOM) [23]. Where concentrations of total soluble surfactants are high, parameterising k_w
64 solely in terms of bulk turbulence may involve significant errors [9, 24].
65
66 Surfactant suppression of k_w by up to 50% may be typical but such estimates are mostly
67 based on artificial compounds used in laboratory experiments[7, 15] and/or deployed at sea [11, 18].
68 In coastal regions, strong spatio-temporal gradients in k_w have been linked to natural
69 surfactants, both in the SML and in the underlying near-surface seawater[8, 24, 25]. We recently
70 found persistent total surfactant activity (SA) enrichments in the Atlantic Ocean SML around
71 40°N and 10°N [9]. Air-sea gas exchange rates estimated for these regions without accounting
72 for such enrichments will almost certainly be too high. Previous estimates of the surfactant
73 effect utilised chlorophyll as a surfactant proxy[17]. We develop this further herein, providing
74 the first direct and systematic evaluation of surfactant suppression of air-sea gas exchange at
75 the ocean basin scale (Atlantic Ocean), based on observed changes in measured SA and in k_w
76 estimated experimentally with our unique laboratory gas exchange tank[26]. Suppression
77 estimates were derived for individual biogeographical ocean provinces ("Longhurst
78 Provinces") defined by phytoplankton distributions as regulated by hydrography[27]. Our gas
79 exchange tank is a proven and effective tool for elucidating the relationships between k_w, SA
80 and biogeochemical indices of primary productivity[26]. The data we present here were
81 obtained along Atlantic Meridional transect (AMT) #24 from 50°N to 50°S during
82 September-November 2014 (Figure 1).
83
84 **Surfactants and gas exchange in the Atlantic Ocean**
85 Our data synthesis sets the Atlantic Ocean contribution to the 2014 global marine CO_2 sink at
86 ~25% (1433 Tg C). Our gas exchange tank experimental results show that in comparison to
87 surfactant-free water used as a control, k_w was suppressed in Atlantic Ocean waters by 2 - 32

% (Table S1), which is generally greater than a previous estimate of 5% suppression for the open ocean [28]. Using sea surface temperature (SST) and salinity as a conservative tracer of Atlantic Ocean water bodies (Figure 1) we found a consistently smaller degree of k_w suppression in the South Atlantic (3-18%) than in the North Atlantic (2-24%), and highest k_w suppressions in the Western Tropical Atlantic (WTRA, 6°S–11°N). We related these results (Table S1 and Figure S1) directly to our previously published measurements of SA in the SML (SA range for all sites used in this study = 0.15 to 0.67 mg L^{-1} T-X-100, n = 13; Table S1) [9] and derived a linear relationship (% suppression = 32.44 x SA_{SML} + 2.51, r^2 = 0.51, p = 0.009, n =13) that is similar to what we previously found for the coastal North Sea [25]. The range in SML SA relevant to our gas exchange tank experiments is comparable to the ranges we reported previously [9] for individual Longhurst Provinces, consistent with our derived relationship for the Atlantic Ocean being representative of the wider SA distribution we observed (Table S2). However, the SA variability that we found within each individual Longhurst Province implies a corresponding variability in province-wide values of k_w, which prompts a need for further gas exchange experiments of this type to reduce the attendant uncertainties. Additionally, we note that the SA vs k_w relations for our North Sea [25] and Atlantic Ocean datasets have contrasting slopes and intercepts. These imply that in addition to differences in the total concentrations of SML surfactants (SA) in these two areas, variability in the chemical compositions of their total surfactant pools will likely impact k_w variability [29]. This brings into question approaches that employ proxies such as chlorophyll-a to quantify the suppression of k_w by surfactants [17], and this is supported by our recent North Sea [25] and Atlantic Ocean [9] datasets that show no clear relationships between SA in the SML and either total chlorophyll, total pigments or size-fractionated primary production.

To further interrogate the effect of surfactants on Atlantic Ocean CO_2 exchange, we adjusted wind-speed derived CO_2 fluxes with an empirically-derived, non-linear % Suppression-SST relationship (r^2 = 0.61, n = 13; see methods, Figure S2, and Table S3). Our estimated mean k_w suppression due to surfactants is spatially and temporally variable (Figure S3) and the wind speed relation of Nightingale et al. [4] that we used to calculate k_w derives from spatially and temporally heterogeneous coastal seas for which no corresponding SA measurements are available. Consequently, the influence of surfactants on its wind speed-derived estimates of k_w are unknown. We note that all available k_w parameterisations [3, 4, 5] are likely derived from data that are influenced by variable SA. We evaluated the percent k_w suppressions by surfactant for each of the three coastal locations included in the Nightingale et al. [4] synthesis (Southern North Sea, Georges Bank, Florida Shelf) by applying our above % suppression-SST relationship to the published temperature ranges for these experiments (5.3-16.9 °C) [4, 30, 31]. The resulting range in k_w suppression was 0.3-6.5 %. We also note that the majority of the data used in the Nightingale et al. [4] analysis (those from the Southern North Sea and Georges Bank) are from locations bordering regions of very low surfactant suppression (Figure S3). Based on this we applied the central limit theorem (see methods) and so assume that the data used to develop the Nightingale et al. [4] parameterisation comprise of an equal number of surfactant-influenced and surfactant-free data points and that the upper range of this surfactant influence is likely low (i.e. <=6.5% suppression). Following this reasoning, the Nightingale et al. [4] relation thus identifies the central estimate of the k_w-wind speed relation, which tends towards surfactant-free conditions. We therefore contend that our use of the Nightingale et al. [4] relation as a reference is entirely reasonable given that this study is the first systematic attempt to evaluate the surfactant effect at the ocean basin scale. We selected SST based on its use in satellite algorithms, in conjunction with photosynthetically active radiation and chlorophyll-a, for estimating primary production integrated over time and

space. This integration has the advantage of smoothing out any process-related time lags that are manifested in the phytoplankton photosynthetic response and subsequent surfactant production [29, 32]. Such time lags are consistent with our inability to observe any clear relationship between SA and chlorophyll-a, and likely account for at least some of the otherwise unexplained variance in our data. Applying this relationship to our experimental and observational results yields a basin-wide, spatio-temporal estimate of the impact of surfactants (see Figure S3). The resulting range in k_w suppression for individual grid-squares (1° x 1°; see methods) was 2 to 24 % and the corresponding net effect on the 2014 Atlantic Ocean CO_2 sink was to reduce it by 9 % (131 Tg C), from 1433 Tg C (derived using wind parameterisation based estimates alone[4]) to 1302 Tg C (Table S3 expressed as R_{660}' values and Table S4), with monthly values of % suppression ranging from 2.6 to 11.2 %, peaking in November (Table S3). Recent work in the Atlantic Ocean between 40°N and 60°N highlighted the importance of bubble-mediated CO_2 exchange during wave breaking at high wind speeds [33, 34]. In our earlier work we found surfactants to be ubiquitous in the Atlantic Ocean SML up to wind speeds of at least 13 m s^{-1} [9], beyond the typical threshold for wave breaking [33], and that the SML surfactant enrichments were maximal between 40°N and the northern boundary of our study at 50°N [9]. A co-existence of bubbles and surfactant in these high wind regions will act to impact air-sea gas exchange in two ways. First, we contend that irrespective of the important solubility-driven enhancement of k_w by bubbles [35], a separate "surfactant effect" at these wind speeds will to some extent attenuate the increase in gas exchange rates that would otherwise be exerted through this bubble effect alone. Second, by coating the surfaces of rising bubbles surfactants act to reduce their rise speeds and thereby force an additional inhibition of air-sea gas exchange [35]. As we have shown previously [25], the influence of surfactants on k_w, whether in the presence of bubbles or not, is spatially and temporally variable, due to corresponding variability in both SA and near-surface turbulence

(e.g. as driven by wind speed), which will also impact bubble production. Consequently, in regions of high and variable winds uncertainty over the fractional contribution of surfactants to k_w will be maximal, being compounded by the presence of bubbles, and both spatially and temporally variant.

We hypothesise that the increases in % suppression we observed for both the North and South Atlantic are in large part likely driven by total sunlight hours that influence primary productivity at the sub-basin scale. If so, the observed temporal variability may be associated with seasonality and/or the movements of air such as the trade winds, and atmospheric moisture and cloud formation in the inter-tropical convergence zone (ITCZ). Partitioning of the total net air-sea CO_2 flux between the North and South Atlantic in our analysis was similar with and without surfactant suppression (54 % vs 46 %). At the Longhurst Province scale there were notable 'hotspots' of CO_2 flux suppression that were sustained throughout the year (Figure 2 and Table S4). The largest reduction was found for the North Atlantic Tropical Gyral (NATR) province, where purely wind-based CO_2 exchange may be overestimated by up to 4.6 Tg C per month, whereas the smallest impact was found for the North Atlantic Subtropical Gyre - West (NAST(W)) and Eastern Tropical Atlantic (ETRA) provinces (0.03 Tg C per month). The most prevalent surfactant effects were in WTRA and NATR and occurred throughout the year, with other hotspots in the North Atlantic Subtropical Gyral – East (NAST(E)) and NAST(W) provinces from October to June (Figure 2). These hotspots imply that at these times the Atlantic Ocean contribution to the global CO_2 sink is reduced by 10-24%. However, when NAST(E) (August-September), NAST(W) (July-September), and ETRA (February-June) all became net CO_2 sources the 'surfactant effect' also reduced CO_2 emissions. Further minor reductions in CO_2 emissions were notable off the

West African coast in June, south of the equatorial Atlantic from January to May and along 30°N from July to October (Figure 2).

Global implications of the surfactant suppression effect

Our analysis shows that SML surfactants impact the air-sea exchange of CO_2 at the oceanic scale. Consequently, spatio-temporal variability in SA and hence in k_w suppression likely accounts for a substantial fraction of the observed uncertainty in basin-wide CO_2 air-sea fluxes. More tightly constraining this suppression and its variability in space and time should therefore aid in reducing the uncertainty inherent in constraining net oceanic CO_2 uptake. The surfactant suppression effect is particularly important given our recent work that suggests a persistence of surfactants in the SML beyond wind speeds at which they were previously thought to disperse [9]. The occurrence of "hotspots" of CO_2 exchange in the Atlantic Ocean during warmer periods, as revealed by our analysis, highlights a need to more effectively constrain the temporal and spatial scales of k_w suppression by surfactant and the distributions of SA and related physical and biogeochemical variables, not only in the Atlantic but in all major ocean basins. Such studies will substantially improve the confidence of CO_2 uptake estimates that we necessarily up scaled from limited data and should lead to the development of more effective proxies for estimating the spatio-temporal variability of surfactant control on air-sea gas exchange.

Specifically, the use of Atlantic Ocean SST as a spatial and temporal integrator of the variability in SA requires additional verification via further measurements in all major ocean basins, where we currently lack any clear supporting evidence of a link between SA and SST or between SA and other potential SA proxies. If SST indeed proves to be a universally robust predictor of SML surfactants resulting from primary production, this would be an

211 important step towards refining the “surfactant suppression effect”. This important positive
212 feedback mechanism to ocean carbon uptake should be taken account of in future evaluations
213 of the global carbon cycle and the attendant implications for future global climate.

References

1. Upstill-Goddard RC. Air–sea gas exchange in the coastal zone. *Estuarine, Coastal and Shelf Science* 2006, **70**(3)**:** 388-404.
2. Asher WE. The effects of experimental uncertainty in parameterizing air-sea gas exchange using tracer experiment data. *Atmos Chem Phys* 2009, **9**(1)**:** 131-139.
3. Ho DT, Wanninkhof R, Schlosser P, Ullman DS, Hebert D, Sullivan KF. Toward a universal relationship between wind speed and gas exchange: Gas transfer velocities measured with $^{3}He/SF_6$ during the Southern Ocean Gas Exchange Experiment. *Journal of Geophysical Research-Oceans* 2011, **116:** C00F04.
4. Nightingale PD, Malin G, Law CS, Watson AJ, Liss PS, Liddicoat MI*, et al.* In situ evaluation of air-sea gas exchange parameterizations using novel conservative and volatile tracers. *Global Biogeochemical Cycles* 2000, **14**(1)**:** 373-387.
5. Wanninkhof R. Relationship between Wind-Speed and Gas-Exchange over the Ocean. *Journal of Geophysical Research-Oceans* 1992, **97**(C5)**:** 7373-7382.
6. Wanninkhof R, McGillis WR. A cubic relationship between air-sea CO_2 exchange and wind speed. *Geophysical Research Letters* 1999, **26**(13)**:** 1889-1892.
7. Bock EJ, Hara T, Frew NM, McGillis WR. Relationship between air-sea gas transfer and short wind waves. *Journal of Geophysical Research-Oceans* 1999, **104**(C11)**:** 25821-25831.
8. Frew NM, Goldman JC, Dennett MR, Johnson AS. Impact of phytoplankton-generated surfactants on air-sea gas-exchange. *Journal of Geophysical Research-Oceans* 1990, **95**(C3)**:** 3337-3352.
9. Sabbaghzadeh B, Upstill-Goddard RC, Beale R, Pereira R, Nightingale PD. The Atlantic Ocean surface microlayer from 50°N to 50°S is ubiquitously enriched in

surfactants at wind speeds up to 13 m s^{-1}. *Geophysical Research Letters* 2017, **44**(6)**:** 2852-2858.

10. Wurl O, Miller L, Vagle S. Production and fate of transparent exopolymer particles in the ocean. *Journal of Geophysical Research-Oceans* 2011, **116:** C00H13.

11. Brockmann UH, Huhnerfuss H, Kattner G, Broecker HC, Hentzschel G. Artificial surface-films in the sea area near Sylt. *Limnology and Oceanography* 1982, **27**(6)**:** 1050-1058.

12. Leck C, Bigg EK. Aerosol production over remote marine areas - A new route. *Geophysical Research Letters* 1999, **26**(23)**:** 3577-3580.

13. Cunliffe M, Engel A, Frka S, Gasparovic B, Guitart C, Murrell JC*, et al.* Sea surface microlayers: A unified physicochemical and biological perspective of the air-ocean interface. *Progress in Oceanography* 2013, **109:** 104-116.

14. Zancker B, Bracher A, Rottgers R, Engel A. Variations of the Organic Matter Composition in the Sea Surface Microlayer: A Comparison between Open Ocean, Coastal, and Upwelling Sites Off the Peruvian Coast. *Frontiers in Microbiology* 2017, **8:** 2369.

15. Goldman JC, Dennett MR, Frew NM. Surfactant effects on air sea gas-exchange under turbulent conditions. *Deep-Sea Research Part a-Oceanographic Research Papers* 1988, **35**(12)**:** 1953-1970.

16. McKenna SP, McGillis WR. The role of free-surface turbulence and surfactants in air-water gas transfer. *International Journal of Heat and Mass Transfer* 2004, **47**(3)**:** 539-553.

17. Tsai WT, Liu KK. An assessment of the effect of sea surface surfactant on global atmosphere-ocean CO_2 flux. *Journal of Geophysical Research-Oceans* 2003, **108**(C4): 3127.

18. Salter ME, Upstill-Goddard RC, Nightingale PD, Archer SD, Blomquist B, Ho DT*, et al.* Impact of an artificial surfactant release on air-sea gas fluxes during Deep Ocean Gas Exchange Experiment II. *Journal of Geophysical Research-Oceans* 2011, **116:** C11016.

19. Wurl O, Holmes M. The gelatinous nature of the sea-surface microlayer. *Marine Chemistry* 2008, **110**(1-2)**:** 89-97.

20. Sieburth JM, Willis PJ, Johnson KM, Burney CM, Lavoie DM, Hinga KR*, et al.* Dissolved organic matter and heterotrophic microneuston in the surface microlayers of the north atlantic. *Science* 1976, **194**(4272)**:** 1415-1418.

21. Lass K, Friedrichs G. Revealing structural properties of the marine nanolayer from vibrational sum frequency generation spectra. *Journal of Geophysical Research-Oceans* 2011, **116:** C08042.

22. Kuznetsova M, Lee C, Aller J, Frew N. Enrichment of amino acids in the sea surface microlayer at coastal and open ocean sites in the North Atlantic Ocean. *Limnology and Oceanography* 2004, **49**(5)**:** 1605-1619.

23. Tilstone GH, Airs RL, Martinez-Vicente V, Widdicombe C, Llewellyn C. High concentrations of mycosporine-like amino acids and colored dissolved organic matter in the sea surface microlayer off the Iberian Peninsula. *Limnology and Oceanography* 2010, **55**(5)**:** 1835-1850.

24. Schmidt R, Schneider B. The effect of surface films on the air–sea gas exchange in the Baltic Sea. *Marine Chemistry* 2011, **126**(1–4)**:** 56-62.

25. Pereira R, Schneider-Zapp K, Upstill-Goddard RC. Surfactant control of gas transfer velocity along an offshore coastal transect: results from a laboratory gas exchange tank. *Biogeosciences* 2016, **13**(13)**:** 3981-3989.

26. Schneider-Zapp K, Salter ME, Upstill-Goddard RC. An automated gas exchange tank for determining gas transfer velocities in natural seawater samples. *Ocean Sci* 2014, **10**(4)**:** 587-600.

27. Longhurst A. Seasonal cycles of pelagic production and consumption. *Progress in Oceanography* 1995, **36**(2)**:** 77-167.

28. Wurl O, Stolle C, Van Thuoc C, Thu PT, Mari X. Biofilm-like properties of the sea surface and predicted effects on air-sea CO_2 exchange. *Progress in Oceanography* 2016, **144:** 15-24.

29. Thornton DCO. Dissolved organic matter (DOM) release by phytoplankton in the contemporary and future ocean. *European Journal of Phycology* 2014, **49**(1)**:** 20-46.

30. Wanninkhof R, Asher W, Weppernig R, Chen H, Schlosser P, Langdon C*, et al.* Gas transfer experiment on Georges Bank using two volatile deliberate tracers. *Journal of Geophysical Research: Oceans* 1993, **98**(C11)**:** 20237-20248.

31. Wanninkhof R, Hitchcock G, Wiseman WJ, Vargo G, Ortner PB, Asher W*, et al.* Gas exchange, dispersion, and biological productivity on the West Florida Shelf: Results from a Lagrangian Tracer Study. *Geophysical Research Letters* 1997, **24**(14)**:** 1767-1770.

32. Hoppe HG, Gocke K, Koppe R, Begler C. Bacterial growth and primary production along a north-south transect of the Atlantic Ocean. *Nature* 2002, **416**(6877)**:** 168-171.

33. Bell TG, Landwehr S, Miller SD, de Bruyn WJ, Callaghan AH, Scanlon B*, et al.* Estimation of bubble-mediated air-sea gas exchange from concurrent DMS and CO_2 transfer velocities at intermediate-high wind speeds. *Atmospheric Chemistry and Physics* 2017, **17**(14)**:** 9019-9033.

34. Blomquist BW, Brumer SE, Fairall CW, Huebert BJ, Zappa CJ, Brooks IM*, et al.* Wind Speed and Sea State Dependencies of Air-Sea Gas Transfer: Results From the

High Wind Speed Gas Exchange Study (HiWinGS). *Journal of Geophysical Research-Oceans* 2017, **122**(10)**:** 8034-8062.

35. Patro R, Leifer I, Bowyer P. Better Bubble Process Modeling: Improved Bubble Hydrodynamics Parameterization. *Gas Transfer at Water Surfaces*. American Geophysical Union, 2013, pp 315-320.

Acknowledgements

AMT director Andy Rees (Plymouth Marine Laboratory) enabled our participation in *JCR* cruise 303 (AMT24) and we thank the crew and scientists who supported our work. We thank the British Oceanographic Data Centre (BODC) for calibrated ancillary data, and Jon Barnes (Newcastle) and Juliane Bischoff (Lyell Centre) for laboratory support and cruise mobilisation. This work was supported by grants from the Leverhulme Trust to RCUG (RPG-303) and the UK Natural Environment Research Council (NERC) to RCUG (NE/K00252X/1) and JDS (NE/K002511/1). Both NERC grants are components of RAGNARoCC (Radiatively active gases from the North Atlantic Region and Climate Change), which contributes to NERC's Greenhouse Gas Emissions and Feedbacks program (www.nerc.ac.uk/research/ funded/programmes/greenhouse). JDS and IA acknowledge additional support from the European Space Agency (grant 4000112091/14/I-LG). RP acknowledges support from Prof. Wagner. This study is a contribution to the international IMBeR project and was supported by the UK NERC National Capability funding to Plymouth Marine Laboratory and the National Oceanography Centre, Southampton. This is contribution number 324 of the AMT programme. Finally, we thank three anonymous reviewers whose comments improved this manuscript.

Contributions

R.P. performed the gas exchange experiments. B.S. provided the surfactant measurements. I.A. and J.D.S developed the FluxEngine analysis and ran the model. R.P. and R.U.G. conceived the study. All authors discussed the results and developed the project and manuscript.

Competing financial interests

The authors declare no competing financial interests

Figures and Figure Captions

Figure 1: Left: Atlantic Meridional Transect 24 (AMT24) from the UK to the Falkland Islands, 2014. The cruise transect (blue line) crosses the following Longhurst Biogeographical Provinces: North Atlantic Drift (NADR); North Atlantic Subtropical Gyral—East (NAST(E)); North Atlantic Subtropical Gyral—West (NAST(W)); North Atlantic Tropical Gyral (NATR); Western Tropical Atlantic (WTRA); Eastern Tropical Atlantic (ETRA); South Atlantic Gyral (SATL); and the South Subtropical Convergence (SSTC). AMT24 start and end shown as blue diamonds. Sample locations shown in black circles. Right: Scatterplot of % suppression of k_w as a distribution of Atlantic Ocean temperature and salinity in 2014.

Figure 2: Monthly maps of the estimated difference in air-water CO_2 flux caused by surfactants. FluxEngine outputs presented as suppressed flux – original flux, with lighter colours showing decreased CO_2 emission and darker colours showing decreased CO_2 uptake.

Methods

Sample Collection

Samples were collected and gas exchange experiments executed during Atlantic Meridional Transect Cruise (AMT) 24 on board R.R.S *James Clark Ross* (*JCR*; Figure 1). The cruise track ran southbound from Immingham, UK to Port Stanley, Falkland Islands, between 22 September and 6 November 2014. The cruise crossed seven biogeographical provinces defined by Longhurst [27]: North Atlantic Drift (NADR, 44–58°N); North Atlantic Subtropical Gyral—East (NAST(E)), 26–44°N); North Atlantic Tropical Gyral (NATR, 11–26°N); Western Tropical Atlantic (WTRA, 6°S–11°N); South Atlantic Gyral (SATL, 42–6°S); and the South Subtropical Convergence (SSTC, 45–42°S).

Sea surface microlayer (SML) and sub-surface water (SSW) samples were collected during midday CTD casts following a well-established protocol [36]. To minimise contamination from *JCR* all samples were collected following best practices detailed in Sabbaghzadeh, et al. [9]. Briefly, the SML was sampled using a Garrett Screen [37] (mesh 16, wire diameter 0.36 mm, opening 1.25 mm), with an effective surface area of 2025 cm^2, transferred to 50 mL high-density polyethylene (HDPE) bottles and stored in an on-board refrigerator at 4 °C [13, 25]. SSW was collected from the ship's underway non-toxic seawater supply (located approximately 3-5 m below the water surface) after flushing of the line with copious amounts of sample seawater. 93 litres of this seawater were directly loaded into our gas exchange tank for gas exchange experiments that commenced immediately and were completed within 1.5 hours of sample collection. 50 mL sample aliquots were also collected in HDPE bottles and stored in an on-board refrigerator at 4 ºC for subsequent SA analysis that was completed within 24 hours. We used SSW in the tank experiments following the procedure outlined by Pereira, et

382 al. [25] as there is no practical procedure for collecting a large volume sample of surface
383 seawater that preserves the integrity of the SML. However, we have shown (i) that following
384 its disturbance by vigorous mixing in a laboratory tank the SML becomes re-established on a
385 time scale of seconds with respect to surfactants and other SML components [13]; (ii) that a
386 new SML is similarly established when sub-surface coastal waters are pumped into large
387 mesocosm tanks [38].
388
389 **Sample Analysis**
390 Surfactant activity (SA) in the SML and in SSW was measured on board *JCR* by phase-
391 sensitive hanging mercury drop AC voltammetry [39] (797 VA Computrace: Metrohm,
392 Switzerland), within 24 hours as previously reported by Sabbaghzadeh, et al. [9]. In brief, the
393 polarograph was situated on a gimbal table to minimise any vibration due to ship movement
394 that might otherwise affect the integrity of the mercury drop. All samples were analysed in
395 triplicate, with their salinities pre-adjusted to 35.0 via the addition of surfactant-free 3 mol
396 L^{-1} NaCl solution or by dilution with Milli-Q 18.2 Ohm deionised water (Millipore System
397 Inc., USA). Calibration was against the non-ionic soluble surfactant Triton T-X-100. The SA
398 of Milli-Q water was continually analysed throughout the cruise and was always found to be
399 below the method detection limit. All equipment was acid-washed (10% HCl) and rinsed in
400 Milli-Q 18.2 Ohm deionised water prior to use.
401
402 The SSW samples were used to estimate the variability in k_w using a fully automated, closed
403 air–water gas exchange tank, the design, operation and routine rigorous cleaning of which are
404 described in detail elsewhere [25, 26]. Briefly, the system generates controllable and
405 reproducible water-side turbulence with an electronically operated baffle whilst measuring
406 the partial pressures of artificially enriched gaseous tracers. To achieve this the gas exchange

407 tank is coupled to two gas chromatographs (GC's) in a continuous gas-tight system, which
408 allows temporal changes in the partial pressures of the gaseous tracers to be measured
409 simultaneously in the tank water (via an integral equilibrator) and headspace, thereby
410 facilitating independent estimates of k_w for each turbulence setting applied. Due to the
411 dependence of k_w on the Schmidt Number (*Sc*: the ratio of kinematic viscosity of water to gas
412 diffusivity**)** raised to the power *n*, the k_w estimates were converted to $k_{660,}$ the value of k_w for
413 Sc = 660 (the value for CO_2 in seawater at 20 °C), assuming n = 0.5 for a wavy surface [1]. The
414 setup of the gas exchange tank system on board *JCR* differed slightly from our previous
415 studies [25] in that only CH_4 and the lowest water-side baffle setting of 0.6 Hz were selected.
416 Using only one tracer gas allowed for simpler setup in a relatively confined space and our
417 previous work demonstrated significantly better analytical precision for CH_4 than for SF_6 [25].
418 With a baffle setting of 0.6 Hz, bubble generation in our gas exchange tank is precluded [25]. A
419 critical consideration of our experimental setup was to account for the movement of the ship,
420 which had the potential to create turbulence additional to that generated in the experiments.
421 We therefore ran a surfactant-free Milli-Q water sample (herein referred to as a sample
422 blank) immediately prior to each seawater sample. The sample blank k_{660} (cm hr^{-1}) was
423 normalised to the k_{660} of an 'installation blank', a surfactant-free Milli-Q water sample that
424 was run whilst the ship was stationary in port prior to the cruise. SA analysis of the Milli-Q
425 water ensured that the gas exchange tank was surfactant-free prior to the experiment. The
426 resulting correction factor was then applied to k_{660} derived for each sample (i.e. $k_{660\ \text{Sample}}$' =
427 $k_{660\ \text{Sample}}$ x ($k_{660\ \text{Installation Milli-Q}}$ / $k_{660\ \text{Sample Milli-Q}}$). To ascertain the comparative SA effect on k_w
428 we normalised our seawater k_{660}' values for each site to the k_{660} value of the installation blank
429 (i.e. R_{660}' = $k_{660\ \text{Sample}}$' / $k_{660\ \text{installation blank}}$) [26]. The uncertainty in each k_{660} measurement was
430 derived via Gaussian error propagation [40] and was always less than ±0.6 cm hr^{-1} (n = 13). To
431 gauge the possibility of artefacts arising from biological production or consumption of CH_4,

from losses due to leakage or arising from GC analytical drift, the total masses of CH_4 were continually estimated over the duration of the experiments, from their measured partial pressures and the known water-phase and air-phase volumes (mass balance; Schneider-Zapp, et al. [26], Eq. 14). All experimental data with a total mass balance error of more than ±5 % were excluded [25].

Supporting biogeochemical and meteorological data were obtained from the AMT data pool, accessible via the British Oceanographic Data Centre (BODC) (http://www.bodc.ac.uk). Physical parameters including *in-situ* salinity and temperature were logged from the ship's underway non-toxic seawater systems and calibrated against discrete samples using benchtop instruments. Wind speed and direction were measured using an on-board meteorological package and post processed following BODC guidelines. Chlorophyll a concentrations were determined on samples collected at 2 m depth from the midday CTD cast, by acetone extraction and fluorometric detection according to Welschmeyer [41].

Ocean - Atmosphere Fluxes

Ocean - atmosphere exchange of CO_2 was calculated using the FluxEngine toolbox, an established set of open-source Python tools that enable user defined inputs and gas flux parameterisations in the estimation of regional and global fluxes [42, 43, 44].

In this work, ocean - atmosphere CO_2 fluxes were calculated following equation 2 of Shutler, et al. [43] and were consistent with the rapid model methods and temperature handling of Woolf, et al. [45]. The wind speed relation of Nightingale, et al. [4] implemented within FluxEngine was used to calculate k_w, such that $k_w = (0.222(U_{10})^2 + 0.333U_{10})\ (Sc/600)^{-1/2}$, where Sc is the Schmidt number of CO_2. Net integrated air-sea CO_2 fluxes were calculated by

457 FluxEngine with adjustments for sea ice (using the ice normalisation of Takahashi, et al. [46]),
458 varying pixel areas (assuming Earth is an ellipsoid) and sub grid cell variations of land and
459 sea as described in Appendix A of Shutler, et al. [43].
460
461 All gas flux calculations used CO_2 fugacity (fCO_2) as inputs and calculated the CO_2
462 concentration at the top and bottom of the mass boundary layer. Earth observation sea surface
463 temperature (SST_{fnd}) data from the Reynolds data set [47] are calibrated to depth and so can be
464 used to represent the temperature at the bottom of the mass boundary layer, allowing the CO_2
465 concentration at this point to be calculated. A constant cool-skin difference of -0.17°C [48] was
466 applied to the SST_{fnd} to represent the skin (interface) temperature SST_{skin}, allowing the CO_2
467 concentration at the top of the mass boundary layer to be calculated.
468
469 Surface-water fCO_2 (fCO_{2W}) data were obtained from the Surface Ocean CO_2 Atlas
470 (SOCAT) version 4 observations. These were re-analysed to a common satellite-derived sea
471 surface temperature (SST) data set that represents the temperature at the bottom of the mass
472 boundary layer [47], using the method of Goddijn-Murphy, et al. [49]. A global climatology,
473 normalised to the year 2010, was then created from these data [49].
474
475 Atmospheric pCO_2 (pCO_{2A}) was calculated by FluxEngine using modelled air pressure (P)
476 from the European Centre for Medium-Range Weather Forecasts (ECMWF) ERA-interim
477 model and the in-situ CO_2 dry air mole fraction (XCO_2) from the National Oceanic and
478 Atmospheric Administration Earth System Research Laboratory (NOAA ESRL) [50]. pCO_{2A}
479 was converted to fCO_{2A} (µatm) using Weiss [51]: equation 9,
480
481 $$b11 = -1636.75 + (12.04SST_{skin} - 0.033{SST_{skin}}^2 + 3.17\mathrm{e}^{-5}{SST_{skin}}^3)$$

$$d12 = 57.7 - 0.12SST_{skin}$$

$$fCO_{2A} = \exp\left[1e^{-6}(b_{11} + d_{12})\left(\frac{P}{R\ SST_{skin}}\right)\right] pCO_{2A}$$

Where the gas constant, R = 82.06, cm^3 atm $(mol\ K)^{-1}$

Global wind speed at 10 m (U_{10}), was taken from the European Space Agency (ESA) GlobWave (GlobWave 2015) data set. The salinity dataset was from the World Ocean Atlas salinity climatology provided in Takahashi, et al. [46] and global percent sea-ice cover data were from the Centre de Recherche et d' Exploitation Satellitaire (CERSAT) Special Sensor Microwave Imager (SSM/I) dataset. Where they were not originally provided as such, input datasets were re-gridded onto a 1° x 1° grid where each grid value was the statistical mean of all contributing data within that cell.

Surfactant suppression effect modelling

The surfactant suppression effect was determined by fitting a non-linear relationship (R_{660}' = 0.0046 x $SST_{skin}^{2.5673}$) to our R_{660}' and SA dataset presented in this manuscript. This approach recognises that at lower temperatures, primary production effects may be less influential than some other processes (e.g. sea ice formation) [52, 53]. As a result, at lower temperatures, the predicted suppression effect is 0.25% below 5 °C and 0.05% below 3 °C. For this study, we did not apply an upper temperature limit but recognise that further work is needed to constrain the threshold and upper limit at which SST ceases to exert a strong control on primary productivity and hence on SA. In our conceptual approach, we assume that SST_{skin} is the driving factor in primary production and thereby influences the presence of surfactants in the SML. For each Longhurst biogeographical province, we applied our R_{660}' suppression factor to the wind parameterisation of Nightingale et al. [4] to estimate the reduction in CO_2

507 flux across the Atlantic Ocean air-sea interface. The wind speed relation of Nightingale et al.,
508 [4] used to calculate k_w, derives from spatially and temporally heterogeneous coastal seas for
509 which no corresponding SA measurements are available and for which the influence of
510 surfactants on k_w are thus unknown. We therefore assume that the effect of SA inherent in the
511 Nightingale et al. [4] data is variable. Consequently, we applied the central limit theorem.
512 Similar assumptions apply when handling 'Type A' uncertainties, i.e. the analysis of N
513 repeated independent measurements of a quantity, as described by the Joint Committee for
514 Guides in Metrology [54]. This suggests that the Nightingale et al. [4] dataset should contain
515 approximately equal numbers of surfactant-free and surfactant influenced data points. We
516 therefore assume that the Nightingale et al. [4] analysis identifies the central estimate of the k_w-
517 wind speed relationship and thus tends towards a condition of a small amount of surfactant
518 influence. Given this, we adopted the Nightingale et al. [4] parameterisation as our reference.
519
520 Uncertainties in the non-linear relationship between SST and R_{660} were estimated as the
521 RMSE of the residuals when fitted to the in-situ measured data. For the power relationship,
522 the errors from the residuals, $dR_{660} = d(e^{SST})$ and so, $dR_{660} = e^{SST} dSST$. The observed
523 variability is likely to be caused by sea-surface conditions that persist spatially. As such, a
524 spatial correlation length would be expected in the variability. This will serve to increase the
525 variability in net-flux estimates as a purely random spatial signal would be largely removed
526 in a spatial total. It follows that the upper limit in uncertainties will arise when the error is the
527 same simultaneously across the entire area considered. In this work, perturbations were
528 drawn at random from dR_{660} for 20 ensemble runs and applied to all values in an area
529 simultaneously. The uncertainty values were calculated as the RMSE of the relevant value
530 across all runs and represent the largest expected uncertainties.
531

Uncertainty in the in-situ R_{660}' / SST relationships could result from the influence of other factors that affect the flux, and which are not accounted for in the above. However, without additional measurements, we chose to use the largest possible uncertainty estimate. Further data and a more detailed understanding of the relationship between R_{660}' and other relevant parameters would likely reduce these uncertainties.

Data Availability

The authors declare that the data supporting the findings of this study are available within the article and its supplementary information files. FluxEngine outputs are available from the corresponding author upon request. Supporting biogeochemical and meteorological data were obtained from the AMT data pool, accessible via the British Oceanographic Data Centre (http://www.bodc.ac.uk). The FluxEngine documentation is available online: http://www.oceanflux-ghg.org/Products/FluxEngine or the open-source code can be downloaded from github (https://github.com/oceanflux-ghg/FluxEngine). Atmospheric air pressure data were obtained from the European Centre for Medium-Range Weather Forecasts (ECMWF) ERA-interim model (http://apps.ecmwf.int/datasets/data/interim-full-daily/levtype=sfc/). The CO_2 dry air mole fraction (XCO_2) data were from the National Oceanic and Atmospheric Administration Earth System Research Laboratory (https://www.esrl.noaa.gov/gmd/ccgg/globalview/co2/co2_intro.html). Global wind speed at 10m (U_{10}) was obtained from the European Space Agency (ESA) GlobWave (GlobWave 2015: http://globwave.ifremer.fr/) data set and the global percent sea-ice cover data were from the Centre de Recherche et d' Exploitation Satellitaire (CERSAT) Special Sensor Microwave Imager (SSM/I) dataset available at http://cersat.ifremer.fr/data/products/catalogue.

556 **Method References**

557 36. Cunliffe M WO, Engel A, Frka S, Landing W, Latif MT, Yang G-P, Zappa C, Upstill-
558 Goddard R, Gasparovic B, Lindroos A, Leal M, Vagle S, Ekau W, Stolle C, Soloviev
559 A, Lass K. Guide to best practices to study the ocean's surface: Marine Biological
560 Association of the United Kingdom; 2014.
561 37. Garrett WD. Collection of Slick-Forming Materials from the Sea Surface. *Limnology*
562 *and Oceanography* 1965, **10**(4)**:** 602-605.
563 38. Cunliffe M, Salter M, Mann PJ, Whiteley AS, Upstill-Goddard RC, Murrell JC.
564 Dissolved organic carbon and bacterial populations in the gelatinous surface
565 microlayer of a Norwegian fjord mesocosm. *Fems Microbiology Letters* 2009,
566 **299**(2)**:** 248-254.
567 39. Cosovic B, Vojvodic V. The Application of AC Polarography to the Determination of
568 Surface-Active Substances in Sea-Water. *Limnology and Oceanography* 1982, **27**(2)**:**
569 361-368.
570 40. Tayler JR. *An introduction to error analysis: the study of uncertainties in physical*
571 *measurements* University Science Books, Sausalito, 1996.
572 41. Welschmeyer NA. Fluorometric Analysis of Chlorophyll-a in the Presence of
573 Chlorophyll-B and Pheopigments. *Limnology and Oceanography* 1994, **39**(8)**:** 1985-
574 1992.
575 42. Ashton IG, Shutler JD, Land PE, Woolf DK, Quartly GD. A Sensitivity Analysis of
576 the Impact of Rain on Regional and Global Sea-Air Fluxes of CO_2. *PLOS ONE* 2016,
577 **11**(9)**:** e0161105.
578 43. Shutler JD, Land PE, Piolle J-F, Woolf DK, Goddijn-Murphy L, Paul F*, et al.*
579 FluxEngine: A Flexible Processing System for Calculating Atmosphere–Ocean

580 Carbon Dioxide Gas Fluxes and Climatologies. *Journal of Atmospheric and Oceanic*
581 *Technology* 2016, **33**(4)**:** 741-756.
582 44. Wrobel I, Piskozub J. Effect of gas-transfer velocity parameterization choice on air-
583 sea CO_2 fluxes in the North Atlantic Ocean and the European Arctic. *Ocean Science*
584 2016, **12**(5): 1091–1103.
585 45. Woolf DK, Land PE, Shutler JD, Goddijn-Murphy LM, Donlon CJ. On the
586 calculation of air-sea fluxes of CO_2 in the presence of temperature and salinity
587 gradients. *Journal of Geophysical Research-Oceans* 2016, **121**(2)**:** 1229-1248.
588 46. Takahashi T, Sutherland SC, Wanninkhof R, Sweeney C, Feely RA, Chipman DW*, et*
589 *al.* Climatological mean and decadal change in surface ocean pCO_2, and net sea–air
590 CO_2 flux over the global oceans. *Deep Sea Research Part II: Topical Studies in*
591 *Oceanography* 2009, **56**(8–10)**:** 554-577.
592 47. Reynolds RW, Smith TM, Liu C, Chelton DB, Casey KS, Schlax MG. Daily high-
593 resolution-blended analyses for sea surface temperature. *Journal of Climate* 2007,
594 **20**(22)**:** 5473-5496.
595 48. Donlon CJ, Minnett PJ, Gentemann C, Nightingale TJ, Barton IJ, Ward B*, et al.*
596 Toward improved validation of satellite sea surface skin temperature measurements
597 for climate research. *Journal of Climate* 2002, **15**(4)**:** 353-369.
598 49. Goddijn-Murphy LM, Woolf DK, Land PE, Shutler JD, Donlon C. The OceanFlux
599 Greenhouse Gases methodology for deriving a sea surface climatology of CO_2
600 fugacity in support of air-sea gas flux studies. *Ocean Science* 2015, **11**(4)**:** 519-541.
601 50. Dlugokencky EJ, P.M. Lang, J.W. Mund, A.M. Crotwell, M.J. Crotwell, Thoning
602 KW. Atmospheric Carbon Dioxide Dry Air Mole Fractions from the NOAA ESRL
603 Carbon Cycle Cooperative Global Air Sampling Network, 1968-2016, Version: 2017-
604 07-28. 2017.

605 51. Weiss RF. Carbon dioxide in water and seawater: the solubility of a non-ideal gas.
606 *Marine Chemistry* 1974, **2**(3)**:** 203-215.
607 52. Bigdeli A, Loose B, Nguyen AT, Cole ST. Numerical investigation of the Arctic ice-
608 ocean boundary layer and implications for air-sea gas fluxes. *Ocean Science* 2017,
609 **13**(1)**:** 61-75.
610 53. Galgani L, Piontek J, Engel A. Biopolymers form a gelatinous microlayer at the air-
611 sea interface when Arctic sea ice melts. *Scientific Reports* 2016, **6:** 29465.
612 54. BIPM (2008). Evaluation of measurement data — Guide to the expression of
613 uncertainty in measurement. JCGM 100:2008

The effect of biological surfactants on air-sea CO_2 exchange in the Atlantic Ocean

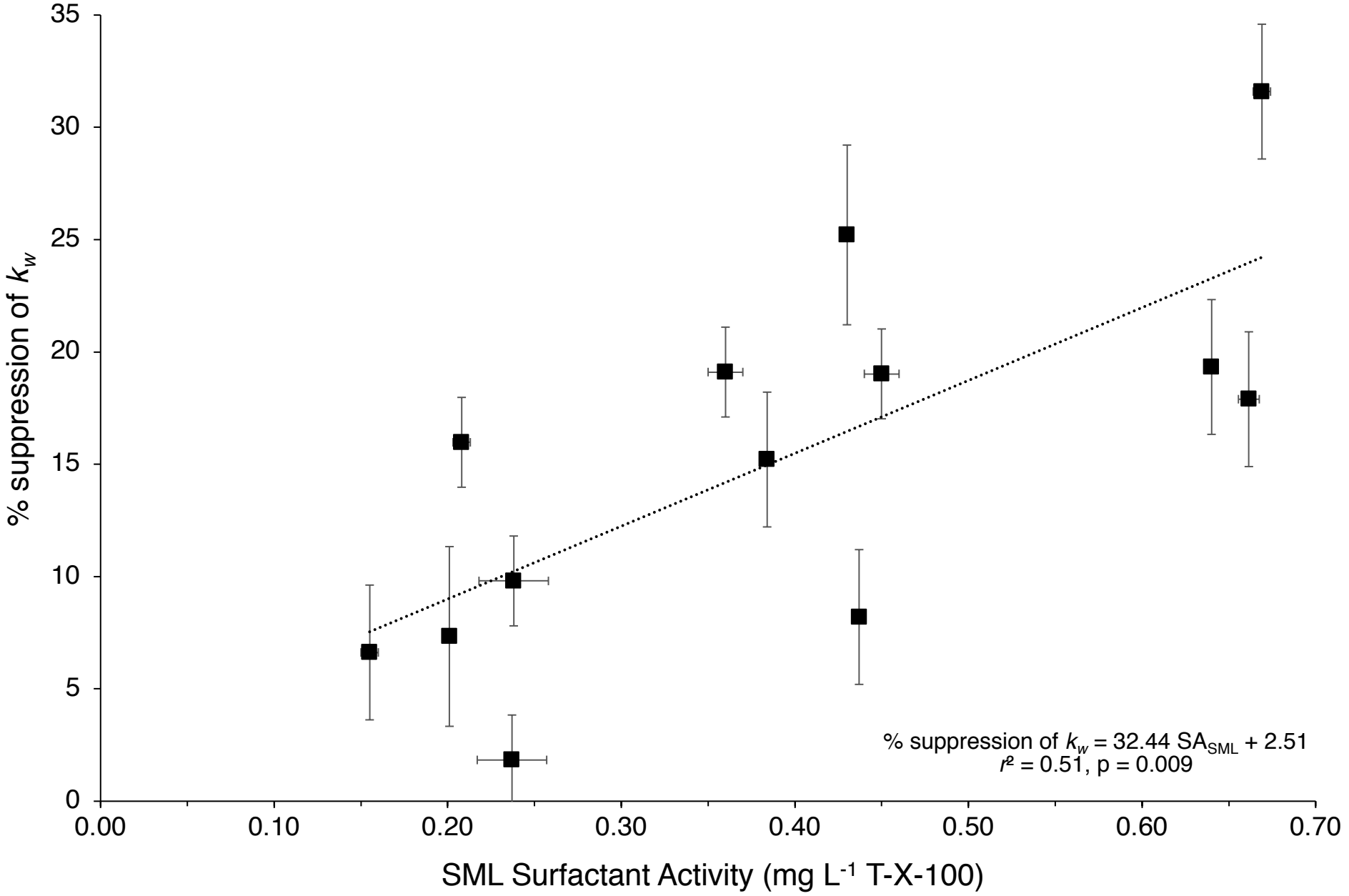

Figure S1: Scatter plot of % suppression of k_w ($R_{660}' = (R_{660}' - k_{660\ Sample}' / k_{660\ installation\ blank})$) and surfactant activity (SA) in the SML for the Atlantic Ocean September to October 2014. Error bars are the standard errors of SA and R_{660}'.

The effect of biological surfactants on air-sea CO_2 exchange in the Atlantic Ocean

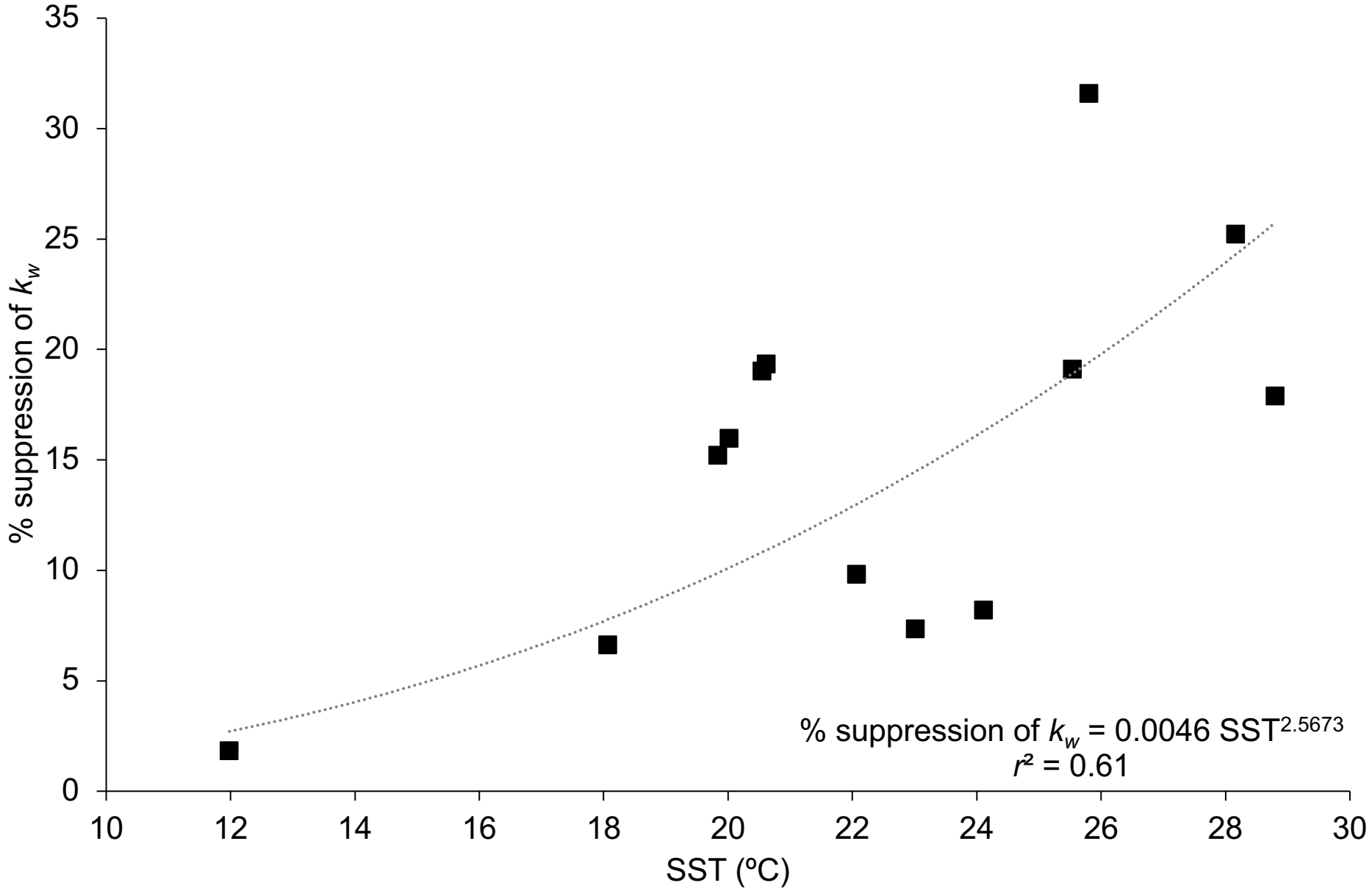

Figure S2: Scatter plot of the SST (°C) and R_{660}' (expressed as % suppression of k_w) non-linear relationship of the Atlantic Ocean from September to October 2014.

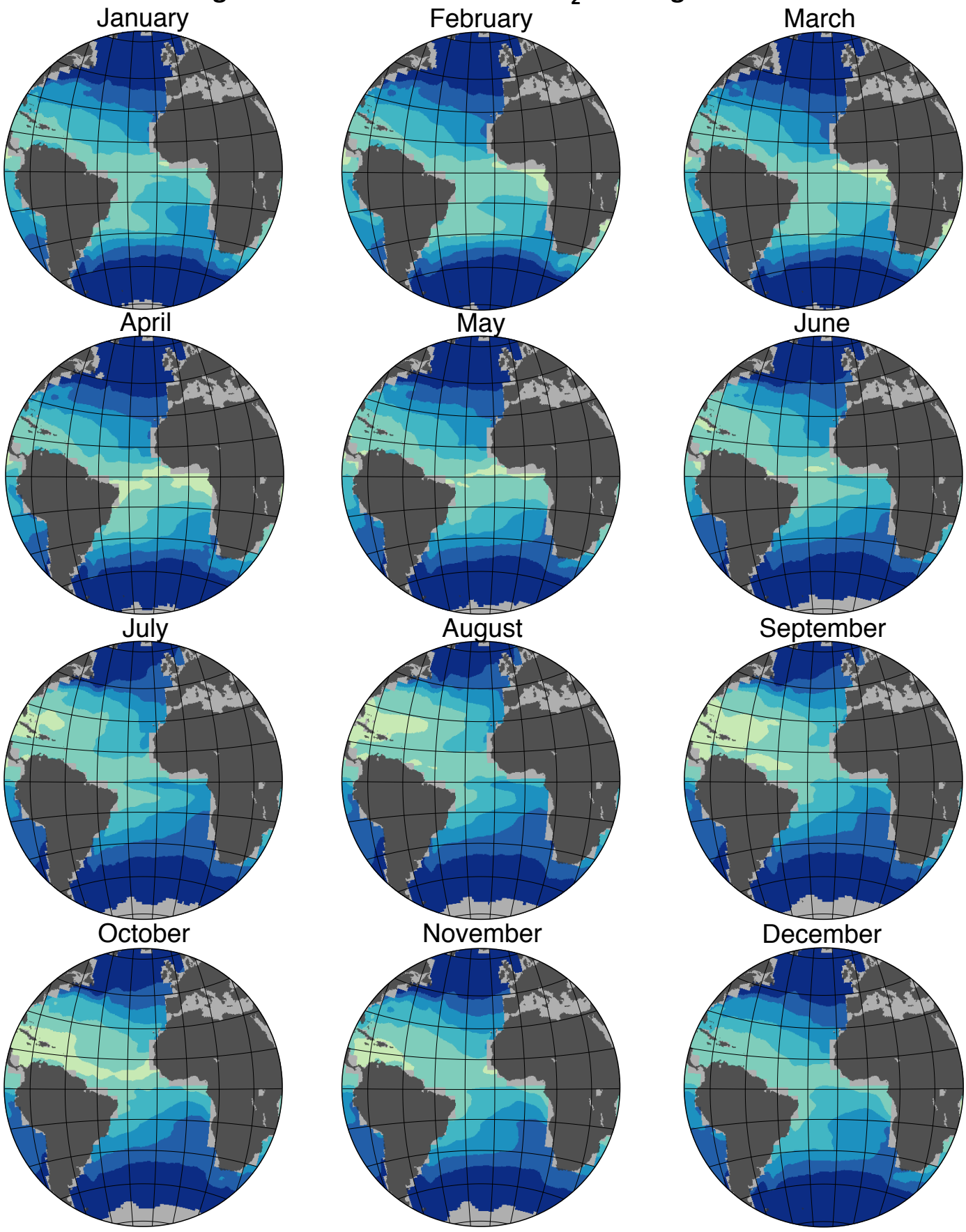

Figure S3: FluxEngine monthly surfactant effect maps of calculated R_{660}' as a function of SST (°C). Light colours show estimates of increased surfactant suppression and darker colours show areas decreased surfactant suppression.